LGD Calibration Update

March 13, 1995

Rob Lindenbusch
Department of Physics, Indiana University, Bloomington IN 47405

1 Introduction

This note describes changes that have been made to the LGD calibration procedure in an attempt to correct known problems. Results from data are compared to Monte Carlo predictions.

2 Motivation

The primary motivation for revising the calibration procedure were the problems with missing masses involving the LGD. These tended to be high, and vary by topology. Sydney did some preliminary work on this, and found that the f_2 MM^2 could be corrected by applying a scale factor of 0.6 to the depth correction. Unfortunatly, this scale factor left the charge exchange η and π^0 masses incorrect (η at 1.2 GeV^2, π^0 at 0.95 GeV^2). Figures 1-3 show the MM^2 for the η, π^0, and f_2 with the full depth correction (scaling the depth correction tends to just scale the MM^2). Clearly something else was going on.

3 The Evidence

The question that was asked was : What makes the charge exchange states differnet from the f_2? Since the photon multiplicity is smaller in the charge exchange states, there are many more high energy photons present in the sample. The MM^2 of the charge exchange π^0's was examined as a function of opening angle. since the assymetry in energy of the photons is a strong function of openning angle. As can be seen in figure 4, the MM^2 is strongly correlated to the π^0 openning angle, ψ. This indicates a possible non-linearity in the detector response.

4 The Correction

At first, a power law non-linearity was attempted, of the form

$$E_{real} = E_{measured}^{\alpha}.$$

The power law has the advantage of a good intuitive physical interpretation, namely the attenuation of the light in the glass. Low energy photons shower earlier, and have there energies undermeasured. This was tried over a wide range of α, and did not solve the problems, unfortunately.

The next form attempted was a logorithmic dependance of the form

$E_{real} = E_{measured} + p_z \alpha \log(E_{real}/E_{critical})$.

This works better, but lacks a good physical interpretation. However, due to it's success, this is the method that has been settled on. The parameter α was tuned to align the π^0, η, and f_2 MM^2 peaks, and then the depth correction was scaled to place these peaks at $0.88 MeV^2$.

Figures 5-7 show the MM^2 for the π^0, η, and f_2 with $\alpha = 0.014$ and the depth correction scaled by 0.8. These can be compared with the Monte Carlo data in fugures 8-10. Note that the Monte Carlo does not behave in the same way as the data. Figure 11 shows the π^0 MM^2 as a function of openeing angle under the new calibration. Although the non-linearity has not been completely removed, it has been reduced. Table 1 compares this result with that of the old calibration.

Opening Angle	Original Calibration	New Calibration
$\psi < 14.8mr$	0.62	0.75
$14.8mr < \psi < 16mr$	0.95	0.93
$16mr < \psi < 20mr$	1.12	1.05
$\psi > 20mr$	1.23	1.15

Table 1. The π^0 MM^2 as a function of opening angle. The data are the ratio of the MM^2 for the given range in opening angle to the MM^2 for all opening angles.

Table 2 shows the MM^2 for the various calibration methods. The current method can probably be tweeked to bring the f_2 anf π^0 MM^2 values more in line. This work is ongoing.

Decay	Original Calibration	Syd's Calibration	New Calibration
$\pi^0 \to \gamma\gamma$	0.73	0.95	0.81
$\eta \to \gamma\gamma$	0.81	1.19	0.95
$f_2 \to \pi^0\pi^0 \to 4\gamma$	0.37	0.87	1.08

Table 2. The mean values of the MM^2, in GeV, for various calibration methods.

Another usefull indicator of the quality of the calibration is the raw energy deposition distribution. Figure 12 shows this for the $\gamma\gamma$ sample with the old and new calibrations. Note that the new calibration has a sharper peak.

5 Masses

Other than the MM^2 and energy, the masses themselves are our best guage of how the calibration is doing. Figures 13-15 show the $\gamma\gamma$ effective masses in the π^0, η, amd η'. Figures 16-19 show the $\pi^0\pi^0$ mass distributions with fits to the K^0 and f_2, using both fitted and unfitted π^0's. Table 3, below, summerizes these results.

Decay		Unfitted	Fitted
$\pi^0 \to \gamma\gamma$	mass (MeV)	133.6	n/a
	σ (MeV)	10.6	n/a
$\eta \to \gamma\gamma$	mass (MeV)	550.8	n/a
	σ (MeV)	25.0	n/a
$\eta' \to \gamma\gamma$	mass (MeV)	977	n/a
	σ (MeV)	25.8	n/a
$f_2 \to \pi^0\pi^0$	mass (MeV)	1292	1305
	σ (MeV)	100	94.5
$K_s^0 \to \pi^0\pi^0$	mass (MeV)	457	501
	σ (MeV)	40	15.9

Table 3. Observed masses for some common particles. A note should be made that the π^0's from f_2's are also observed to be low in mass, and this leads to the increase in f_2 mass observed with the fitter.

6 Conclusions

The new calibration scheme seems to do a better job than the old one. This is seen in the MM^2 distributions for different states and in the dependence of the pi^0 MM^2 on ψ. There are still improvements to be made, and this scheme is not claimed to be the correct scheme, just the best to date. Work will continue both on this method and on exploring other methods.

The other major result of this work is that the Monte Carlo does not behave in the same way as the data. This will need to be explored more, as it seems unlikely at this time that there will be agreement between the two when the final calibration method is arrived at.

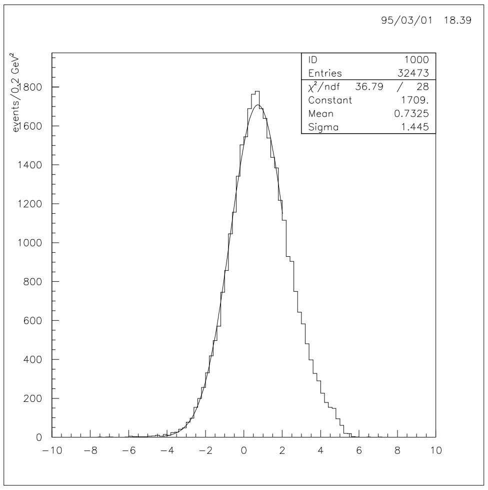

Figure 1. The π^0 MM^2 for the original calibration, with the full depth correction.

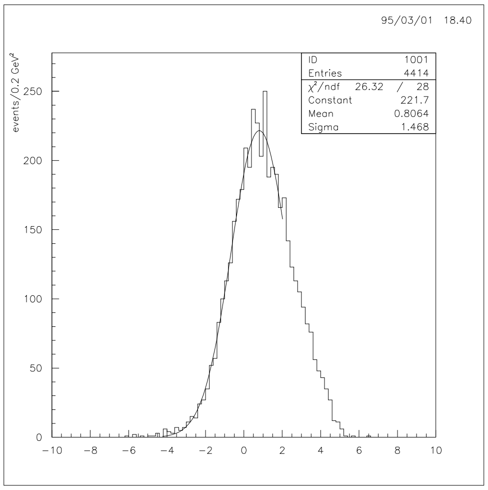

Figure 2. The η MM^2 for the original calibration, with the full depth correction.

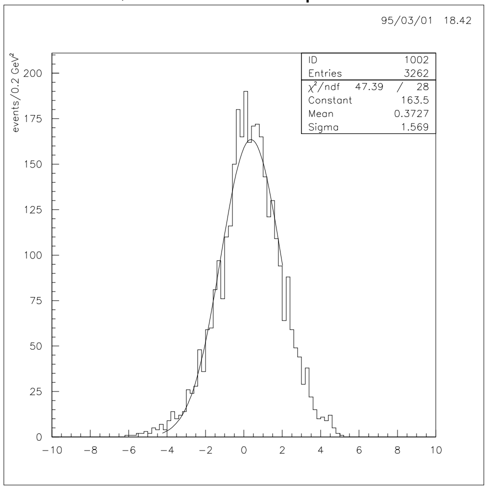

Figure 3. The f_2 MM^2 for the original calibration, with the full depth correction.

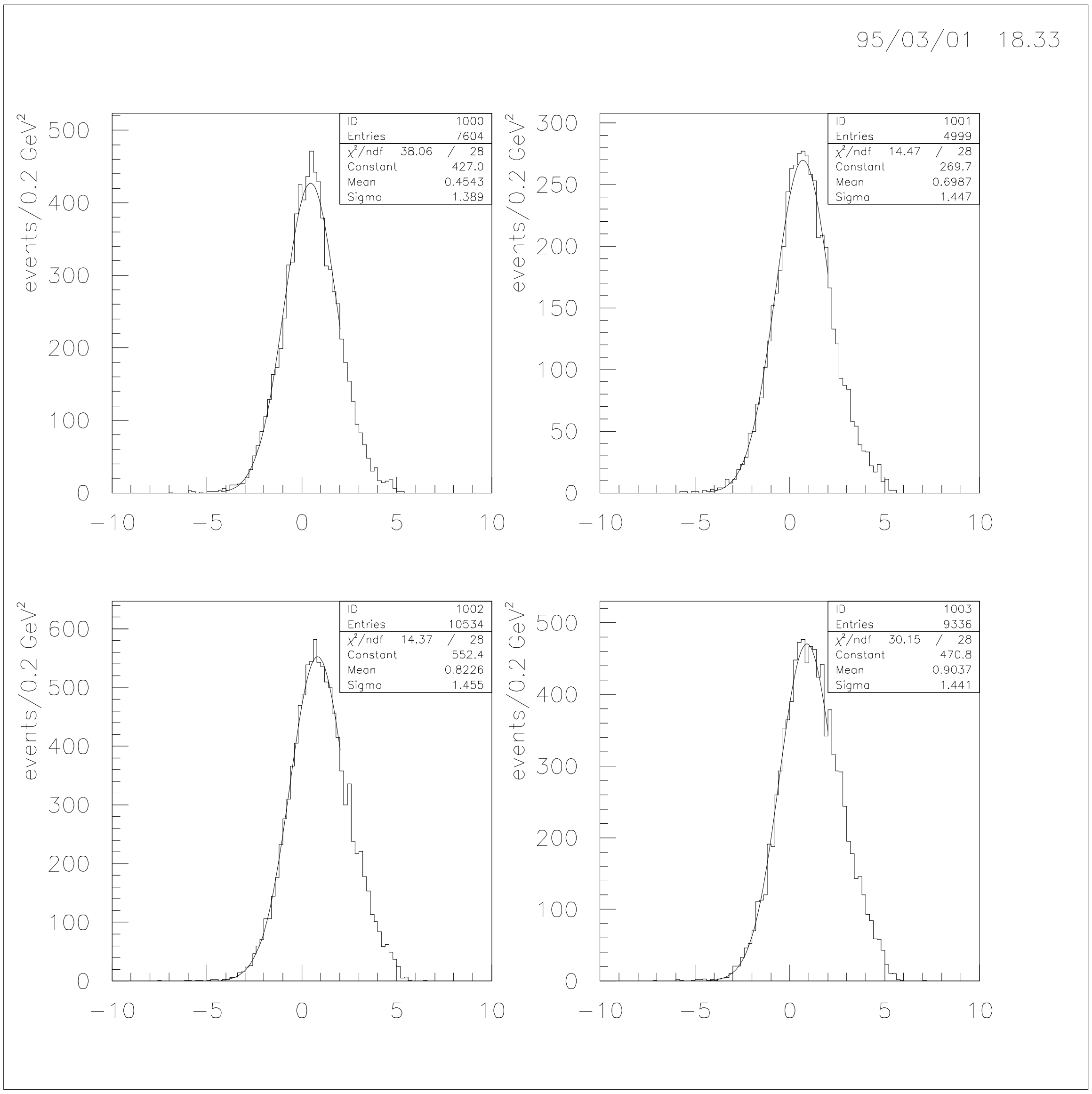

Figure 4. π^0 MM^2 as a function of opening angle, ψ, for the origanal calibration, with the full depth correction. ID 1000 is for $\psi < 14.8mr(\psi_{min})$. ID 1001 if for $14.8mr < \psi < 16mr$. ID 1002 if for $16mr < \psi < 20mr$. ID 1003 is for $\psi > 20mr$.

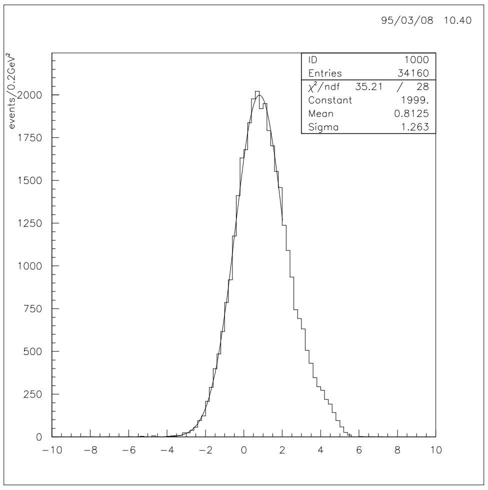

Figure 5. The π^0 MM^2 for the new calibration.

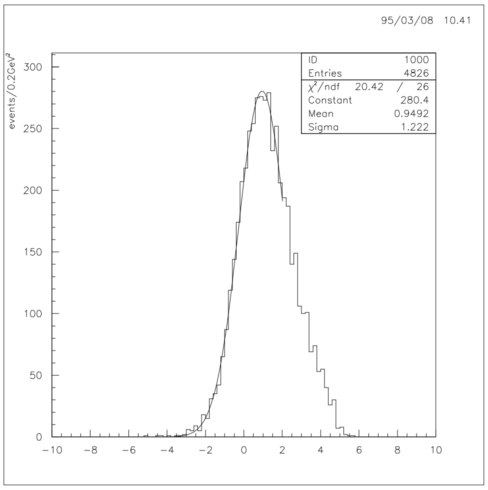

Figure 6. The η MM^2 for the new calibration.

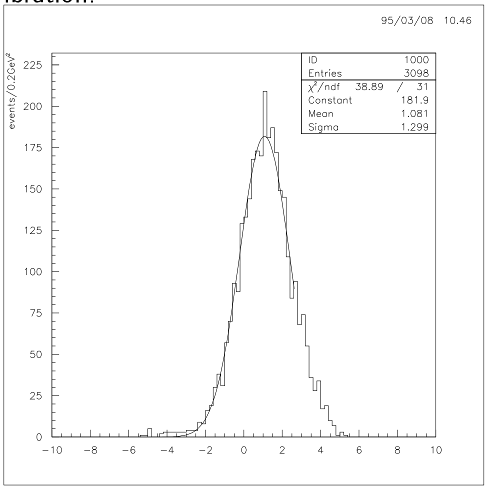

Figure 7. The f_2 MM^2 for the new calibration.

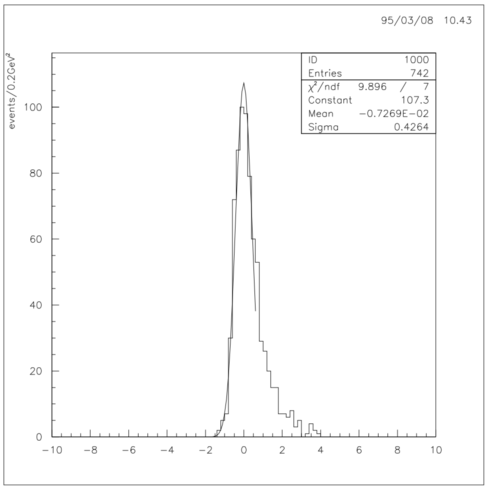

Figure 8. The Monte Carlo π^0 MM^2 for the new calibration.

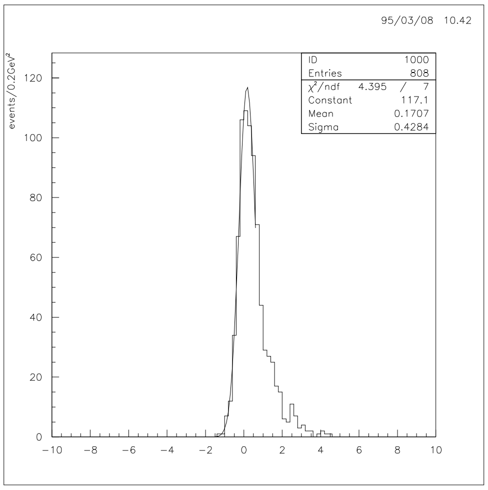

Figure 9. The Monte Carlo η MM^2 for the new calibration.

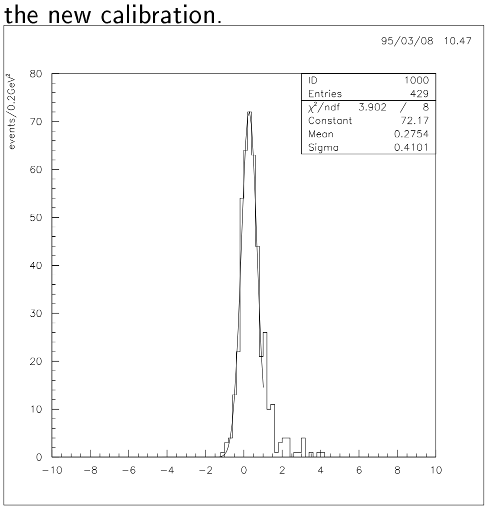

Figure 10. The Monte Carlo f_2 MM^2 for the new calibration.

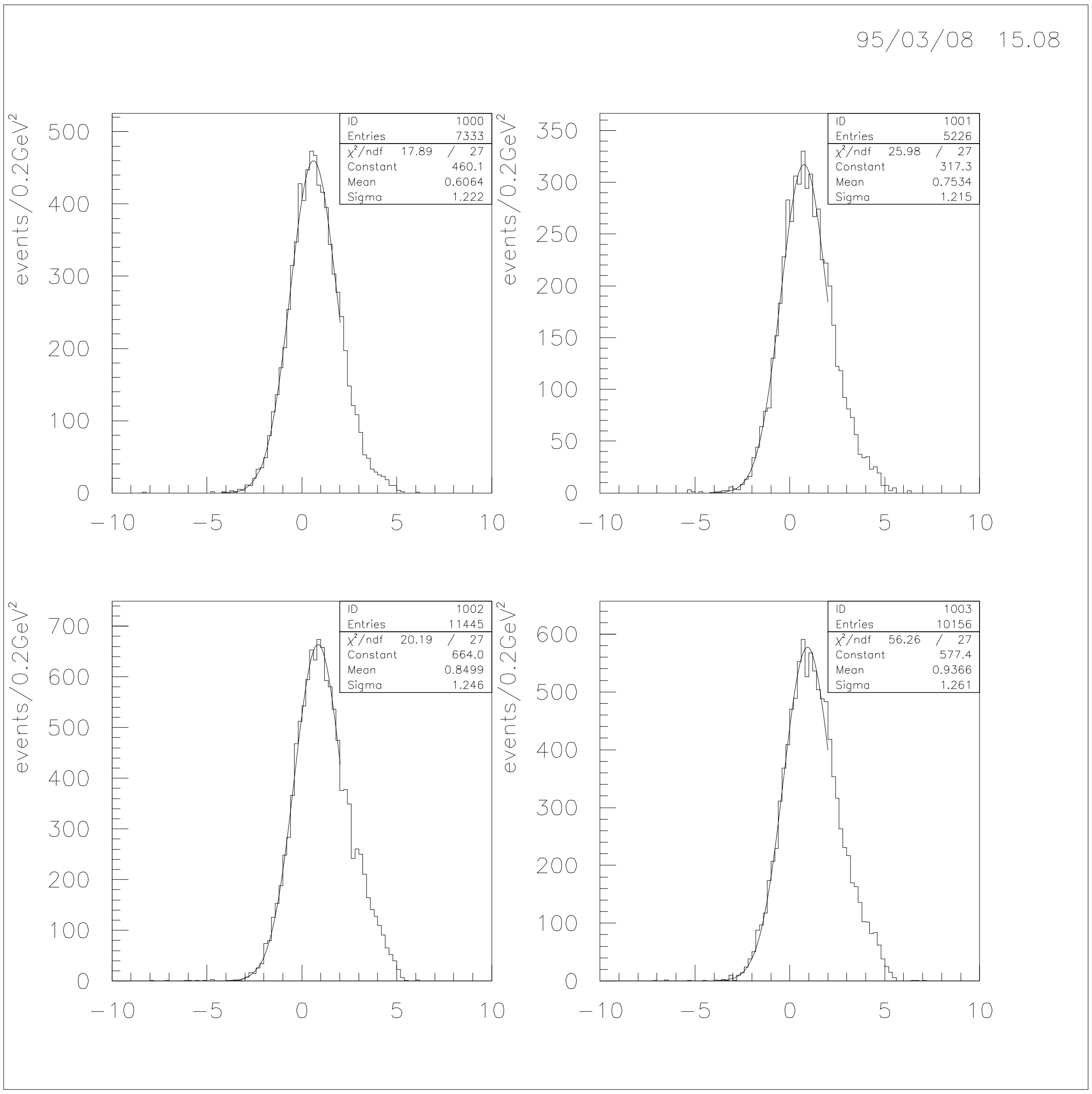

Figure 11. π^0 MM^2 as a function of opening angle, ψ, for the new calibration. ID 1000 is for $\psi < 14.8mr(\psi_{min})$. ID 1001 if for $14.8mr < \psi < 16mr$. ID 1002 if for $16mr < \psi < 20mr$. ID 1003 is for $\psi > 20mr$.

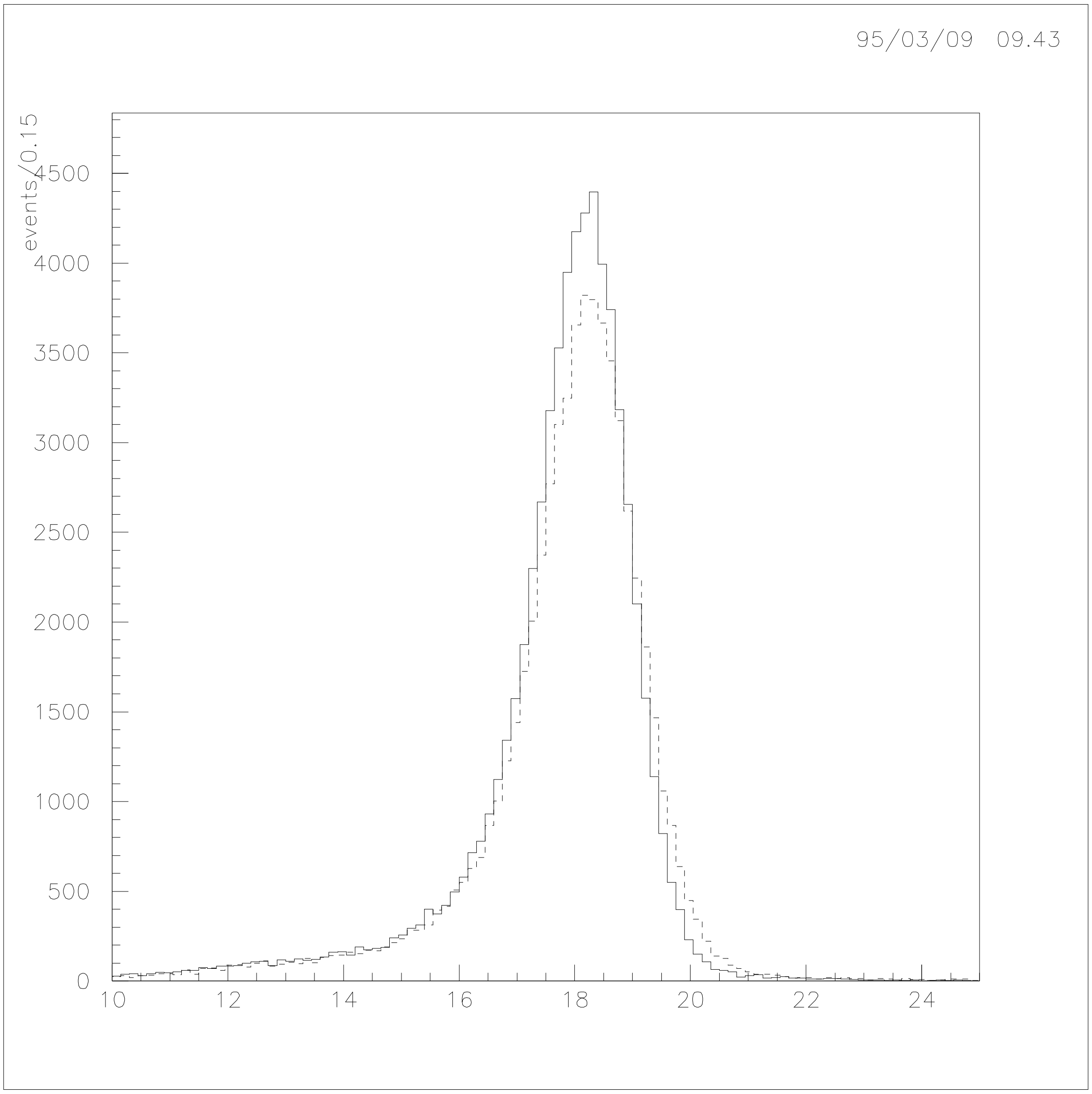

Figure 12. Energy distribution for $\gamma\gamma$ events. The solid line is the new calibration and the dashed is the old.

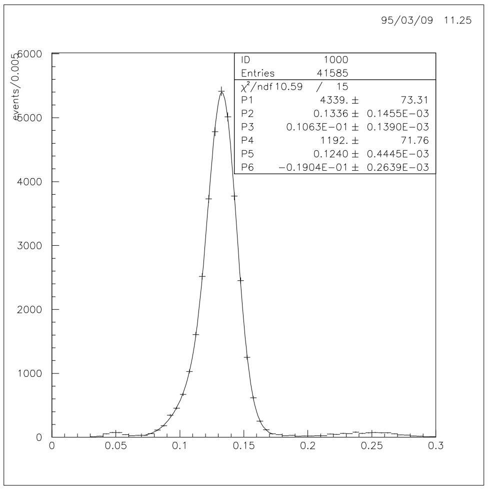

Figure 13. $\pi^0 \to \gamma\gamma$ for the new calibration. The fit is to a double gaussian.

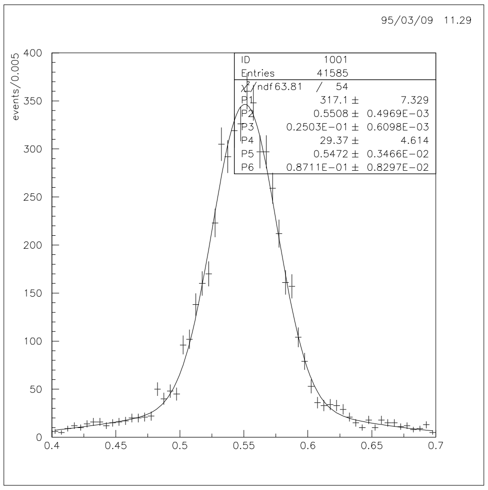

Figure 14. $\eta \to \gamma\gamma$ for the new calibration. The fit is to a double gaussian.

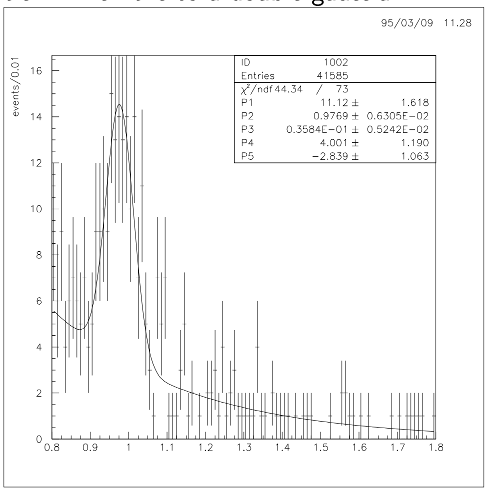

Figure 15. $\eta' \to \gamma\gamma$ for the new calibration. The fit is to a gaussian plus an axponential.

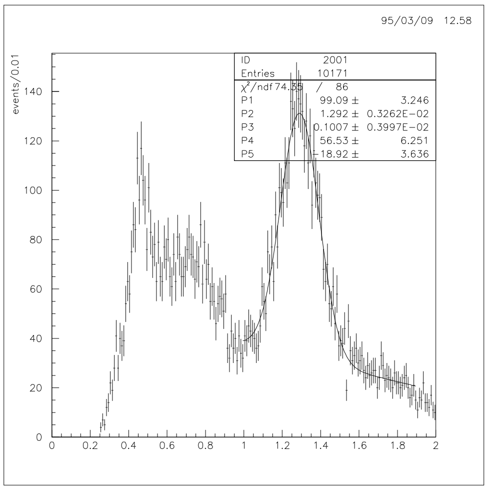

Figure 16. $f_2 \to \pi^0\pi^0$ for the new calibration, unfitted. The fit is to a gaussian plus a line.

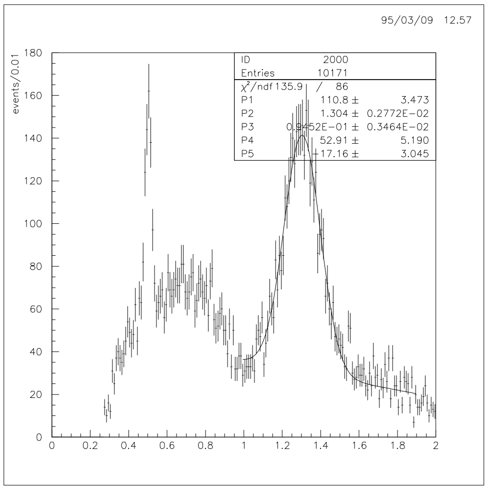

Figure 17. $f_2 \to \pi^0\pi^0$ for the new calibration, fitted. The fit is to a gaussian plus a line.

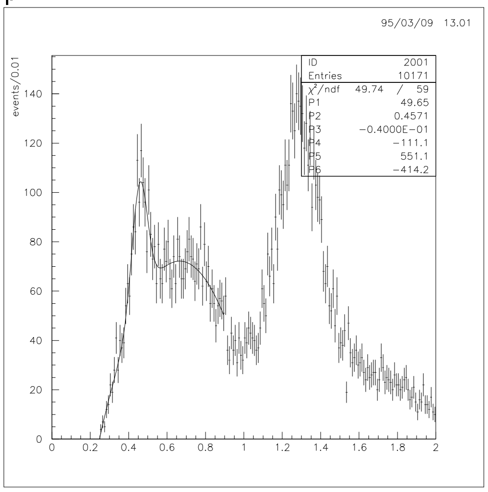

Figure 18. $K_s^0 \to \pi^0\pi^0$ for the new calibration, unfitted. The fit is to a gaussian plus a quadratic.

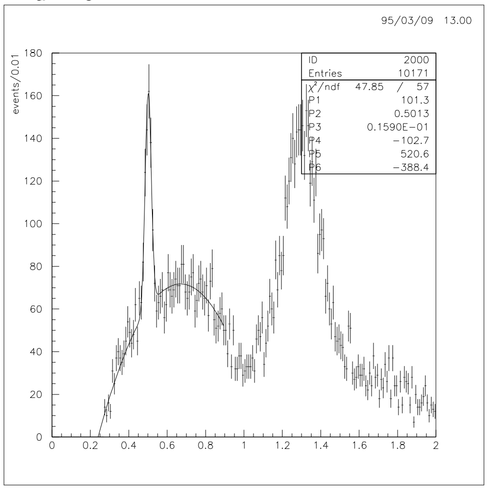

Figure 19. $K_s^0 \to \pi^0\pi^0$ for the new calibration, fitted. The fit is to a gaussian plus a quadratic.